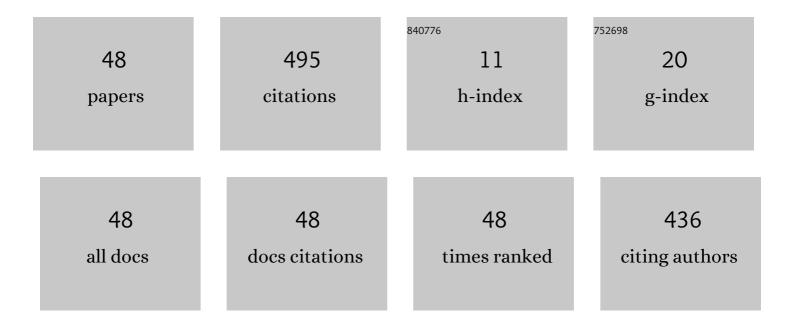
Yusuke Daiko

List of Publications by Year in descending order

Source: https://exaly.com/author-pdf/6612891/publications.pdf Version: 2024-02-01



YUSUKE DAIKO

#	Article	IF	CITATIONS
1	Proton Conduction and Pore Structure in Solâ~'Gel Glasses. Chemistry of Materials, 2002, 14, 4624-4627.	6.7	66
2	Pore size effect on proton transfer in sol–gel porous silica glasses. Microporous and Mesoporous Materials, 2004, 69, 149-155.	4.4	45
3	Dynamics of Proton Transfer in the Solâ^'Gel-Derived P2O5â^'SiO2Glasses. Journal of Physical Chemistry B, 2001, 105, 4653-4656.	2.6	44
4	Remarkable High Proton Conducting P2O5-SiO2 Glass as a Fuel Cell Electrolyte Working at Sub-Zero to 120.DEG.C Journal of the Ceramic Society of Japan, 2001, 109, 815-817.	1.3	40
5	Hydrogen sensor prepared using fast proton-conducting glass films. Sensors and Actuators B: Chemical, 2006, 120, 266-269.	7.8	24
6	Fabrication and thermal conductivity of highly porous alumina body from platelets with yeast fungi as a pore forming agent. Ceramics International, 2016, 42, 13882-13887.	4.8	21
7	Mechanochemically induced sulfur doping in ZnO via oxygen vacancy formation. Physical Chemistry Chemical Physics, 2017, 19, 13838-13845.	2.8	21
8	Deposition of Ultrathin Nafion Layers on Sol–Gel-Derived Phenylsilsesquioxane Particles via Layer-by-Layer Assembly. Journal of the Electrochemical Society, 2008, 155, B479.	2.9	16
9	Structures and electrical properties of core–shell composite electrolytes with multi-heterointerfaces. Solid State Ionics, 2007, 178, 621-625.	2.7	15
10	Formation of Micro and Mesoporous Amorphous Silica-Based Materials from Single Source Precursors. Inorganics, 2016, 4, 5.	2.7	12
11	Low temperature <i>in situ</i> formation of cobalt in silicon nitride toward functional nitride nanocomposites. Chemical Communications, 2021, 57, 2057-2060.	4.1	12
12	The state of P Onb non-bridging oxygen and proton incorporation in binary MO·P2O5 (M = Ca, Mg) phosphate glasses. Solid State Ionics, 2013, 245-246, 19-23.	2.7	11
13	Amine-functionalized polycarbosilane hybrids for CO2-selective membranes. Journal of the European Ceramic Society, 2017, 37, 5213-5221.	5.7	11
14	Formation of a High Conductivity Fuel Cell Electrolyte by Pressing Diphenylsiloxane-Based Inorganic-Organic Hybrid Particles. Journal of the American Ceramic Society, 2009, 92, S185-S188.	3.8	9
15	H+ emission under room temperature and non-vacuum atmosphere from a sol–gel-derived nanoporous emitter. Journal of Sol-Gel Science and Technology, 2017, 83, 252-258.	2.4	9
16	Synthesis of a Novel Polyethoxysilsesquiazane and Thermal Conversion into Ternary Silicon Oxynitride Ceramics with Enhanced Thermal Stability. Materials, 2017, 10, 1391.	2.9	9
17	A hydrostable mesoporous γ-Al2O3 membrane modified with Si–C–H organic-inorganic hybrid derived from polycarbosilane. Journal of Membrane Science, 2020, 598, 117799.	8.2	9
18	Hydrophobicity of amorphous silica-based inorganic-organic hybrid materials derived from perhydropolysilazane chemically modified with alcohols. Microporous and Mesoporous Materials, 2015, 215, 183-190.	4.4	8

Yusuke Daiko

#	Article	IF	CITATIONS
19	High-temperature shrinkage suppression in refractory ceramic fiber board using novel surface coating agent. Ceramics International, 2018, 44, 16725-16731.	4.8	8
20	Proton Incorporation, Mixed Alkaline Effect and H+/e^ ^minus; Mixed Conduction of Phosphosilicate Glasses and Glass-ceramics. Electrochemistry, 2014, 82, 901-905.	1.4	7
21	Palmâ€Sized Ag ⁺ Ion Emission Gun Operated at Room Temperature in Nonâ€Vacuum Atmosphere. Advanced Engineering Materials, 2018, 20, 1800198.	3.5	7
22	Preparation and Fuel Cell Property of a Phosphosilicate Glass with Proton Transport Number tH = 1 at 400–500°C. Electrochemical and Solid-State Letters, 2011, 14, B63.	2.2	6
23	Proton conduction in nanopores of sol–gel-derived porous glasses and thin films. Journal of Sol-Gel Science and Technology, 2014, 70, 172-179.	2.4	6
24	Ag+ ion emission from a sharp Ag2O-Al2O3-P2O5-SiO2 glass-fiber emitter. Solid State Ionics, 2018, 322, 5-10.	2.7	6
25	Hydrogen transport property of polymer-derived cobalt cation-doped amorphous silica. Inorganic Chemistry Frontiers, 2021, 8, 90-99.	6.0	6
26	Proton conduction in glasses prepared via sol–gel and melting techniques. Journal of the Ceramic Society of Japan, 2013, 121, 539-543.	1.1	5
27	Polymer-derived amorphous silica-based inorganic–organic hybrids having alkoxy groups: intermediates for synthesizing microporous amorphous silica materials. Journal of the Ceramic Society of Japan, 2015, 123, 732-738.	1.1	5
28	Synthesis and characterization of organoamine-functionalized amorphous silica materials for CO ₂ -selective membranes. Journal of the Ceramic Society of Japan, 2015, 123, 779-784.	1.1	5
29	Characterization of porous alumina bodies fabricated by high-temperature evaporation of boric acid with sodium impurity. Ceramics International, 2018, 44, 3678-3683.	4.8	5
30	Novel hydrogen chemisorption properties of amorphous ceramic compounds consisting of p-block elements: exploring Lewis acid–base Al–N pair sites formed in situ within polymer-derived silicon–aluminum–nitrogen-based systems. Journal of Materials Chemistry A, 2021, 9, 2959-2969.	10.3	5
31	Indentation-induced stress distribution and pressure effect on the resistivity of YSZ. Solid State Ionics, 2016, 286, 96-101.	2.7	4
32	Microporosity and CO2 Capture Properties of Amorphous Silicon Oxynitride Derived from Novel Polyalkoxysilsesquiazanes. Materials, 2018, 11, 422.	2.9	4
33	Formation and Thermal Behaviors of Ternary Silicon Oxycarbides derived from Silsesquioxane Derivatives. Materials, 2019, 12, 1721.	2.9	4
34	Dynamics of proton infiltration into binary MO·P2O5 (M = Ca, Sr) phosphate glasses. Solid State Ionics, 2019, 335, 151-155.	2.7	4
35	Fluoride ion field emission from a ZBLAC glass emitter. Solid State Ionics, 2020, 353, 115400.	2.7	4
36	Kinetic analysis of crystallization of zeolite beta synthesized by direct heating. Journal of the American Ceramic Society, 2021, 104, 1178-1187.	3.8	4

Yusuke Daiko

#	Article	IF	CITATIONS
37	High-pressure (GPa) impedance measurements based on an indentation-induced local stress field. Solid State Ionics, 2014, 254, 6-10.	2.7	3
38	Growth mechanism of house-of-cards aggregates of alumina platelets containing Na2O–B2O3–SiO2 glass flux. Ceramics International, 2020, 46, 9109-9118.	4.8	3
39	Fabrication of highly isotropic porous alumina refractory clinkers consisting of platelets using a gelatin-sol. Journal of Asian Ceramic Societies, 2020, 8, 265-276.	2.3	3
40	Characterization of anisotropic gas permeability and thermomechanical properties of highly textured porous alumina. Journal of the American Ceramic Society, 2022, 105, 6335-6344.	3.8	3
41	Hydrogen Selective SiCH Inorganic–Organic Hybrid/γ-Al2O3 Composite Membranes. Membranes, 2020, 10, 258.	3.0	2
42	Gas permeation and thermomechanical properties for macroporous alumina focused on necking size at grain boundaries. International Journal of Applied Ceramic Technology, 2022, 19, 828-837.	2.1	2
43	Polymer-derived organoamine-functionalized amorphous silica materials for CO ₂ capture. Journal of the Ceramic Society of Japan, 2016, 124, 989-995.	1.1	1
44	Improvement in heat resistivity of alkaline earth silicate fiber boards by Al ₄ SiC ₄ coating. International Journal of Applied Ceramic Technology, 2019, 16, 2316-2321.	2.1	1
45	Void Formation/Elimination and Viscoelastic Response of Polyphenylsilsesquioxane Monolith. Materials, 2018, 11, 846.	2.9	0
46	Fabrication and characterization of a novel lightweight adiabatic refractory composite consisting of alkaline earth silicate fibers and SiC particles. Ceramics International, 2019, 45, 23248-23255.	4.8	0
47	Reversible Redox Property of Co(III) in Amorphous Co-doped SiO2/Î ³ -Al2O3 Layered Composites. Materials, 2020, 13, 5345.	2.9	0
48	Hydrogen adsorption and electronic structural calculation of a polymer-derived SiCH membrane with a unique affinity for molecular hydrogen. Journal of Sol-Gel Science and Technology, 0, , .	2.4	0